ELSEVIER

Catalysis Today 33 (1997) 205–214

CATALYSIS TODAY

Photoassisted catalytic oxidation of alcohols and halogenated hydrocarbons with amorphous manganese oxides

Jie Chen [a], Jung Chou Lin [b], Vandana Purohit [a], Michael B. Cutlip [b], Steven L. Suib [a,b,c,*]

[a] *U-60, Department of Chemistry, University of Connecticut, Storrs, CT 06269-3060, USA*
[b] *Department of Chemical Engineering, University of Connecticut, Storrs, CT 06269-3060, USA*
[c] *Institute of Materials Science, University of Connecticut, Storrs, CT 06269-3060, USA*

Abstract

This manuscript discusses the synthesis of Amorphous Manganese Oxide (AMO) materials that are used for efficient photoassisted catalytic oxidation of alcohols and halogenated hydrocarbons. Characterization studies suggest that oxygen is lost from AMO very readily under illumination, creating oxygen vacancies that may be important in photooxidation reactions. Alcohols are converted to ketones such as acetone from isopropanol with 100% selectivity at room temperature. These AMO systems have turnover numbers that are over one order of magnitude greater than TiO_2 systems for isopropanol oxidation and over an order of magnitude greater than for TiO_2 systems in decomposition of halogenated hydrocarbons. In addition the TiO_2 systems are poisoned much faster than the AMO materials, especially in degradation of halogenated hydrocarbons. The same high activity and selectivity occur for the total oxidation of halogenated hydrocarbons such as methyl bromide which is converted into CO_2, H_2O and Br_2. The synthesis, characterization, and photoactivity of these materials will be discussed. AMO photocatalysts are also active in the decomposition of methyl choride and methyl iodide.

Keywords: Photooxidation; Alcohols; Halogenated hydrocarbons; Manganese oxide

1. Introduction

When molecules absorb light, energy contents can be markedly enhanced. Excited state species can carry out chemical changes that are not possible in the ground state. An advantage of such excited state reactivity is the ability to store energy in a longterm process by converting light energy to chemical energy [1,2].

Excited state species often last very briefly on the order of nanoseconds or even picoseconds necessitating the need to carry out simple and fast chemical transformations. Electron transfer is a specific example of such reactions that could be exploited in solar energy conversion and storage of energy. A specific example of solar energy conversion which is based on light-induced electron transfer is photosynthesis which occurs in green plants and bacteria [3,4].

Photosynthetic systems have several components that each have a certain responsibility for reaction to take place. Antenna molecules absorb photons and transmit them by energy trans-

* Corresponding author.

PII S0920-5861(96)00119-8

fer processes to the reaction center where actual light-induced electron transfer reactions occur [5,6].

Separation of stable species from highly reactive radical oxidants and reductants is one of the major roles of a photosynthetic system which occur in a series of complex steps. Back reactions and the need to store energy used for metabolism in plants or animals lead to a complex process with energy losses at each step. Photosynthesis is a relatively inefficient process with respect to changing light energy into a chemical product [7,8].

Efficient artificial photosynthetic or photocatalytic systems [9–11] that could be used to convert light energy into stored chemical energy then might be expected to be simply constructed. The ability to transfer charge throughout the system might be another requirement. If the material itself could absorb light rather than using another system as an antenna, efficiency might be enhanced. For these reasons we have been investigating the use of mixed valent manganese oxide materials [12] that are strong absorbers in photoassisted catalytic oxidations of organic molecules such as alcohols [13] and halogenated hydrocarbons [14–16].

Illuminated semiconductors like TiO_2 have appropriate chemical potentials to oxidize organic pollutants into benign products such as CO_2 and H_2O [14,23,26]. Such semiconductors need to have surface sites that can adsorb reactant species such as the organic pollutant, O_2, and H_2O in order to catalyze such reactions [14,23,26]. TiO_2 in the anatase crystal structure is one of the most active materials due to its ability to adsorb oxygen and transform it into superanion radicals, to conversion of adsorbed water into hydroxyl groups, and to the oxygen vacancies created during photolysis which allow adsorption [14,23,26]. Most studies have focused on aqueous solutions of organics.

Few recent studies have focused on photoassisted catalytic oxidation of organic pollutants in the gas phase [14,23,26]. O_2 and H_2O vapor are still necessary to activate gaseous organic pollutants over TiO_2. It is difficult to optimize reactor designs for enhanced activity since differences in light intensity, surface active sites, and partial pressures of reactant gases may depend on the nature of the gaseous pollutant [14,23,26].

The complexities of different reactor systems have led to empirical correlations of data from a variety of laboratories and the results suggest that such photoassisted catalytic oxidations are quite promising for destruction of both aqueous and gas phase pollutants [14,23,26]. Optimization of catalyst properties such as surface area, composition, particle size, chemical potential, light absorbing properties, structure, and morphology is one of the major thrusts of research in this area [14,23,26].

This paper describes the use of mixed valent amorphous manganese oxide (AMO) materials that have been used to oxidize isopropanol to acetone, and in the total oxidation of methyl halides to carbon dioxide. The synthesis and characterization of AMO and doped AMO systems are described. The band gap of AMO is 0.2 eV and occurs near the infrared region. Rates of photooxidation are related to the types of catalysts used, the role of light, the atmosphere used during reaction, absorption spectra, and thermodynamic properties of the reactants. We label these reactions as photoassisted catalytic oxidations since without light there is little or no conversion suggesting that excited state species are important in such reactions.

2. Experimental

2.1. Preparation of amorphous manganese oxide

Potassium permanganate and oxalic acid were added together in a redox type of reaction in order to precipitate amorphous manganese oxide (AMO). Eighty ml of a $KMnO_4$ solution (0.01 M) was added to 100 ml of a 0.25 M oxalic acid solution which led to an exothermic reaction. A

dark brown precipitate is formed in a period of 30 min. The precipitate is washed with distilled deionized water, filtered in a sintered glass filter, and then dried at 110°C for 8h.

2.2. Characterization of AMO materials

The AMO materials were characterized with scanning electron microscopy (SEM), X-ray powder diffraction (XRD), Fourier transform infrared (FTIR) spectroscopy, temperature programmed desorption (TPD), UV–visible (UV–VIS) reflectance spectroscopy, and other methods. SEM experiments were done by mounting AMO powder onto an SEM holder and loading samples into an Amray model 1810 D SEM with energy dispersive X-ray (EDX) analysis capabilities.

X-ray powder diffraction experiments were done on a Scintag Model PDS-2000 theta diffractometer with Cu $K\alpha$ radiation. Experiments were done at 45 kV and 40 mA conditions. Samples were sprinkled onto glass slides and diffraction patterns were collected at 2 degrees 2-theta per minute.

FTIR experiments were done on a Nicolet Magna Model 750 spectrometer. Diffuse reflectance experiments were done with a DTGS detector of KBr with a diffuse reflectance attachment.

TPD experiments were done on a home-made apparatus consisting of a tubular reactor that contained 10 mg of sample. Samples were heated in a furnace at a rate of 15 K/min with He gas as a carrier gas. Oxygen was evolved from the samples and detected with a thermal conductivity detector in a Varian Model 1400 gas chromatograph. The signal from the detector was sent to a Hewlett Packard Integrator model 3396, series 2 which was also interfaced to an IBM personal computer for data storage and analysis. Note that water was isolated in a cold trap so that the analysis by the TCD was only for desorbed O_2.

Diffuse reflectance data were collected on a Hewlett Packard instrument with a Labsphere attachment for diffuse reflectance. The samples were mixed in a 1:10 ratio of sample to $BaSO_4$ which was used as a reference.

2.3. Photoassisted catalytic oxidation of isopropanol

The type of reactor that was used for the selective oxidation of isopropanol to acetone is shown in Fig. 1. The reactor consists of either a stainless steel or glass reactor which has windows for illumination of the catalyst. A 1000 W Xe lamp is used for all photolyses. The light from the lamp is filtered through a water bottle to eliminate infrared radiation from the source as well as through a glass cutoff filter that allows radiation above a wavelength of 420 nm into the reactor via mirrors. The inlet and outlet lines of the reactor are heated with heating tape during reaction in order to minimize condensation of reactant and product. Thermocouples were used to monitor the temperature of the catalyst during photolysis. The catalyst rests on a Gelman Sciences glass fiber filter in a thin layer (15 mg). Products can be trapped in a cold trap with liquid nitrogen or are passed directly into the gas chromatograph through a gas sampling valve. The feed is 1% isopropanol which was transported with an O_2 carrier gas.

A ferrioxalate actinometer was used to measure the intensity of the incident light. The photon flux was measured at 4.6×10^{-7} einsteins per min.

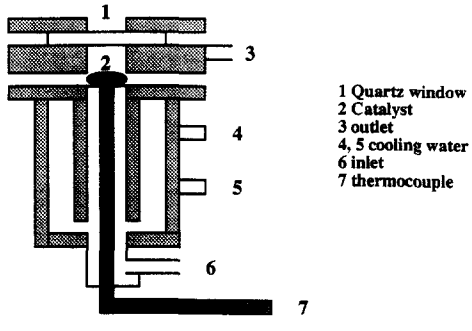

Fig. 1. Diagram of photocatalytic reactor.

2.4. Photoassisted decomposition of halogenated hydrocarbons

A very similar reactor to that used in the selective photoassisted catalytic oxidation of isopropanol was used for total oxidation of methyl halides. Oxygen was used as a diluent (0.5 mol fraction) of the methyl halide/N_2 feed mixtures. Concentrations of CH_3Cl, CH_3Br, and CH_3I were close to 5,000 ppm. Exactly 100 mg catalyst was used. The flow rate was 20 ml/min. A Poropak Q column was used for all gas chromatography experiments and both flame ionization and thermal conductivity detectors were used in order to separate all of the halogenated hydrocarbons, CO, CO_2 and H_2O. The HX and X_2 concentrations were determined by standard titration methods such as with KI.

2.5. Dopant studies

Several dopants such as Cu^{2+}, Cr^{3+}, Ni^{2+} and Zn^{2+} were added to the original AMO synthesis by adding dopant levels of the corresponding metal ion nitrate (2.0×10^{-5} M) to the $KMnO_4$ solution before mixing with the oxalic acid solution. The dopant level concentrations were monitored with inductively coupled plasma (ICP) analysis and are reported in Table 2. The doped AMO materials were studied by a variety of methods including X-ray powder diffraction, scanning electron microscopy, UV–VIS diffuse reflectance spectroscopy, thermogravimetric analysis, and other methods. Doped AMO materials were also studied in photoassisted catalytic oxidations of isopropanol.

2.6. Surface area measurements

The Brunauer, Emmett and Teller (BET) surface area measurements were done with an Omnisorp 100CX analyzer. Surface areas based on the BET equation were calculated with software provided with the Omnisorp instrument.

3. Results

3.1. Preparation and characterization of amorphous manganese oxide

The AMO materials have X-ray powder diffraction patterns similar to that shown in Fig. 2. Note that there are no strong reflections for crystalline materials. Scanning electron microscopy data show that the particle size of the AMO is on the order of 1 μ. Energy dispersive X-ray analysis shows that there are 3 major elements present, K, Mn and O. The dopant concentrations of doped AMO are given in Table 2. The dopant levels are on the order of less than 0.1% by weight. An overall composition of AMO is $K_{0.6}Mn_{0.93}O_2$.

The morphology of the AMO particles is irregular. FTIR data for AMO show bands at 320, 345, 430, 1600 and a series of broad bands at 3,000 to 3,600 cm^{-1} as shown in Fig. 3. In general, most of the bands are rather broad. Diffuse reflectance UV–VIS experiments show a broad absorption ranging from near 350 to 700 nm. These UV–VIS data are very broad with maximum intensity near 400 nm and show a tailing off of absorption into the visible region, finally tapering off near 700 nm.

Temperature programmed desorption data for AMO for photolysis under N_2 and O_2 are shown in Fig. 4. Data for TPD of AMO in N_2 show a major loss of O_2 near 550K and less loss be-

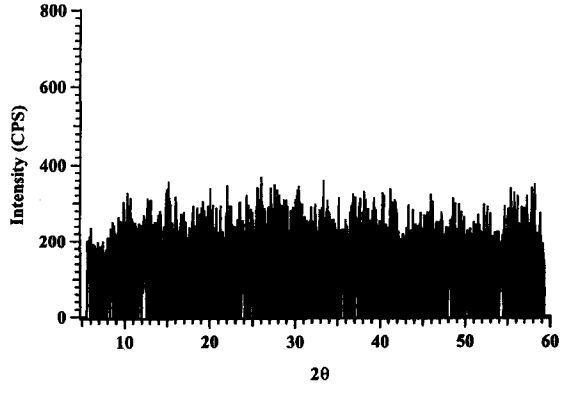

Fig. 2. X-ray powder diffraction of AMO.

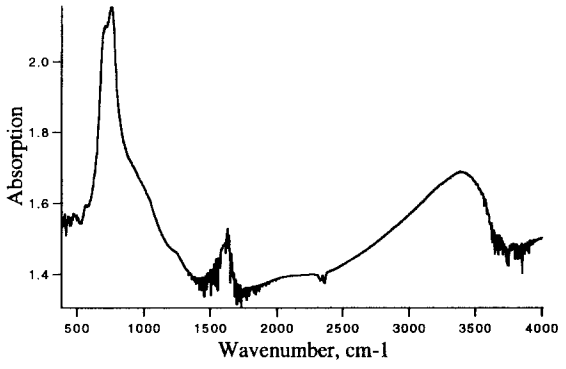

Fig. 3. Fourier transform infrared spectrum of AMO.

tween 600 to 1,000 K. Data for TPD of AMO in O_2 show a loss of O_2 near 520K and an equal amount of loss near 900 K. There is less O_2 loss between 600 and 800 K. The surface areas of AMO and doped AMO materials are on the order of 200 ± 10 m^2/g. The average manganese oxidation states of AMO and doped AMO are on the order of 3.5 to 3.6.

3.2. *Photoassisted catalytic oxidation of isopropanol*

A comparison of the catalytic oxidation of isopropanol in N_2 versus O_2 is given in Fig. 5. Note that the rate of production of acetone from isopropanol is much greater in O_2 than in N_2.

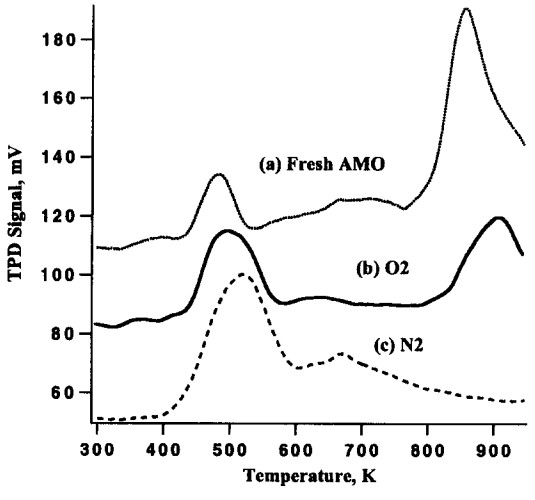

Fig. 4. TPD data for AMO with He carrier gas during photolysis: (a) in N_2; (b) in O_2.

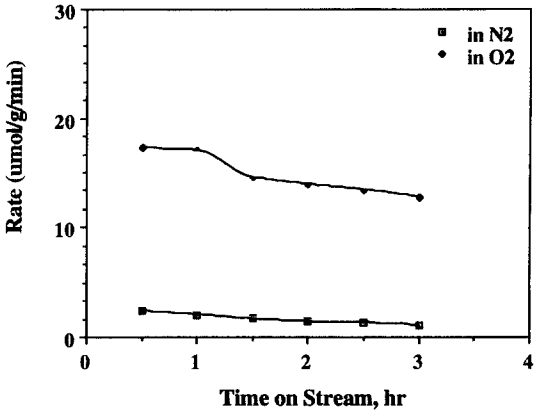

Fig. 5. Photoassisted catalytic oxidation of isopropanol with AMO catalyst: (a) in N_2; (b) in O_2.

The rate initially is 17.3 μmol/g-min and gradually decreases to a value of 12.8 μmol/g-min after a period of 180 min. Blank reactions show a conversion of 0.4% for AMO in the dark and 0% for photoreactions without any AMO. Comparison of the turnover rate of AMO with respect to Degussa P25 TiO_2 shows an enhanced rate for AMO by a factor of 21 even when the TiO_2 material is photolyzed at 350 nm rather than the 425 nm irradiation of AMO. The temperature of the photolyzed AMO is near 45°C during photolysis. Thermal experiments carried out at 45°C show no conversion of isopropanol.

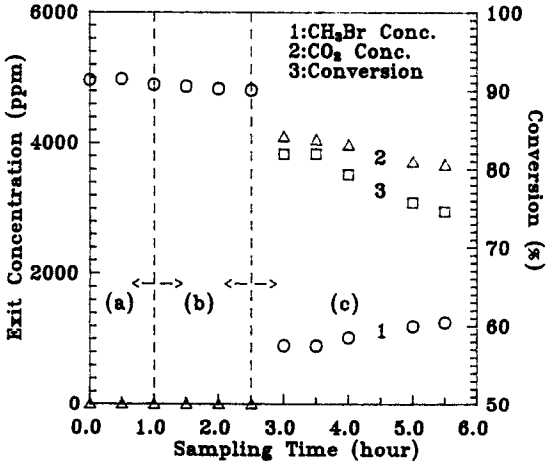

Fig. 6. Photoassisted catalytic oxidation of methyl halides with AMO catalyst: (a) CH_3Cl; (b) CH_3Br; (c) CH_3I.

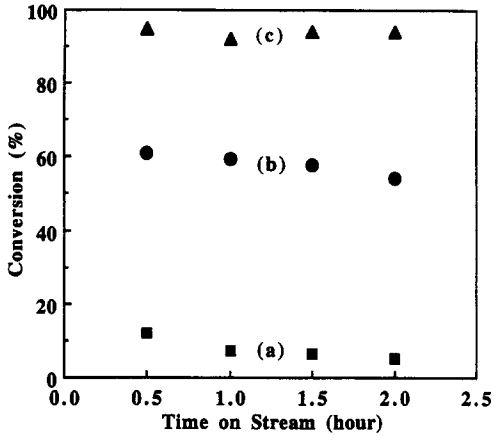

Fig. 7. Photoassisted catalytic oxidation of methyl bromide with AMO catalyst: (a) bypass of reactor; (b) dark reaction; (c) photo reaction.

3.3. Photoassisted decomposition of halogenated hydrocarbons

A comparison of the photoassisted catalytic decomposition of various methyl halides at 5,000 ppm is shown in Fig. 6 for an applied power of 840 W. Note that the rate of decomposition of CH_3I is much greater than that of CH_3Br which in turn is much greater than CH_3Cl. In the absence of O_2 gas (under N_2), the rate of decomposition is considerably lower, on the order of 18% of the rate in the presence of O_2. A plot of conversion for the bypass, in the reactor in the dark and in the reactor in the light is shown in Fig. 7 for an applied power of 1500 W. There is no conversion either in the bypass of the reactor or in the dark at room temperature, whereas conversion occurs in the presence of light. Blank experiments in the absence of AMO catalyst show no activity. These data suggest that there are no homogeneous reactions taking place.

Table 1
Rates of photoassisted catalytic oxidation of methyl halides

Feed	Turnover rate [a]
CH_3Cl	3.11×10^{-6}
CH_3Br	2.38×10^{-5}
CH_3I	3.83×10^{-5}

[a] Turnover rate is defined as the number of moles of CH_3X consumed per gram of AMO per minute.

Thermal temperatures during photolysis are on the order of 70°C. Thermal experiments done at 74°C show a rate of decomposition close to 10%, which is more than 8 times lower than that done under photolysis conditions. It is clear that a photochemical mechanism predominates.

A summary of the different turnover rates of

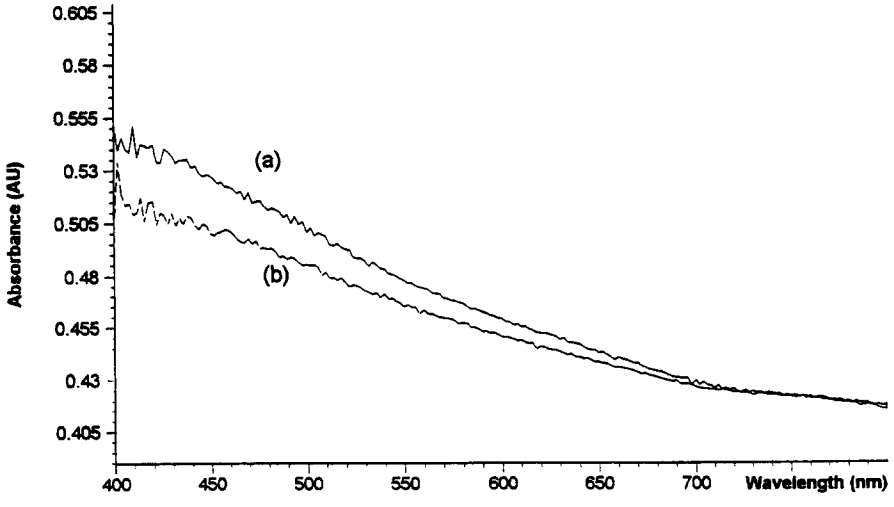

Fig. 8. Diffuse reflectance UV–VIS data for (a) undoped AMO, (b) Zn^{2+} Doped AMO.

CH_3Cl, CH_3Br and CH_3I are shown in Table 1. These data are for inlet concentrations of 5,000 ppm. For comparison purposes, data were collected with a variety of TiO_2 materials including Degussa P25 which had an activity which was 15 times less than AMO. The most active TiO_2 material (sol gel preparation from our laboratory) had lower activity than AMO by a factor of 6. Note that all TiO_2 materials were photolyzed with light of wavelength 320 nm and lower, whereas the AMO was photolyzed with light of wavelength 425 nm.

3.4. Dopant studies

The doped AMO materials have similar colors as the undoped AMO material. X-ray powder diffraction data for all doped materials show no sharp crystalline peaks indicative of crystalline phases. Diffuse reflectance UV–VIS data for undoped and Zn^{2+} doped AMO are shown in Fig. 8. The UV–VIS data show very similar absorption to the other doped AMO materials. As the spectra illustrate, the Zn^{2+} material absorbs more light at longer wavelengths in a relative sense than the undoped material. ICP data show that dopant levels of metal dopants were detected in the solid materials after synthesis with concentrations ranging from 111 ppm (for Cu) to 1072 ppm (for Cr).

A summary comparing the different turnover rates of AMO and doped AMO materials is given in Table 2. These turnover rates range from values of 2.13 mol acetone per total mol Mn per 8 h of photolysis to values of 3.28 mol acetone per total mol Mn per 8 h of photolysis.

Table 2
Turnover rates of photoassisted catalytic oxidation of isopropanol

Catalyst	Dopant concentration [a]	Turnover rate [b]
AMO	a	3.12
Cu^{2+} doped AMO	1.85×10^{-4}	3.28
Cr^{3+} doped AMO	2.21×10^{-3}	1.88
Ni^{2+} doped AMO	8.09×10^{-4}	2.60
Zn^{2+} doped AMO	1.38×10^{-3}	2.13

[a] Ratio of dopant to total manganese concentration.
[b] Mol acetone/mol total Mn — 8 h, ±0.02.

4. Discussion

4.1. Preparation and characterization of amorphous manganese oxide

The reaction of $KMnO_4$ with oxalic acid leads to a redox reaction where the Mn^{7+} state is reduced primarily to Mn^{4+}, with some reduction to Mn^{3+}. This degree of reduction can be controlled by the $KMnO_4$/oxalic acid ratio in the synthesis. The average manganese oxidation state can be determined by thiosulfate titrations as has been done for crystalline octahedral molecular sieves [17] and layered materials [18]. The resulting precipitates are amorphous as shown by the X-ray powder diffraction data of Fig. 2. The SEM data show that there is little regular morphology of the AMO particles. Corresponding energy dispersive X-ray analyses and ICP microanalyses show that some K^+ is incorporated into the AMO materials due to reduction of some of the Mn^{4+} to Mn^{3+}. For every Mn^{3+} there must be a K^+ for charge compensation. This charge compensation mechanism is very similar to that of crystalline octahedral molecular sieves [19].

The FTIR data of Fig. 3 show that there are several bands in the far infrared portion of the spectrum such as at 320, 345, 430 cm^{-1} which are due to Mn–O interactions. The band at 1600 and the series of broad bands at 3,000 to 3,600 cm^{-1} are due to C–H, and C–C vibrations which result from small amounts of unreacted oxalic acid in the final product. Thermal treatment of AMO leads to elimination of these bands and CO_2 can be detected as a product of the thermal treatment by gas chromatography methods.

The absorption spectra of AMO materials show a broad strong band centered near 400 nm. There is considerable intensity at lower wavelengths near 300 nm perhaps indicative of

charge transfer bands [20] in these systems. The dark color of the samples and the broad absorption is in line with the mixed valency of these materials.

Temperature programmed desorption data for AMO in N_2 versus O_2 such as those of Fig. 4 show that surface oxygen can be retained in AMO when a partial pressure of O_2 is used. Oxygen is necessary to regenerate the oxygen that is depleted during photolysis. Kung [21] has suggested that there are several types of oxygen that can desorb from metal oxides such as molecularly adsorbed oxygen, adsorbed atomic oxygen, and lattice oxygen which is evolved at high temperatures. The data of Fig. 4 are in line with this suggestion, where lattice oxygen is evolved near 800K.

The nature and origin of the peak for desorbed oxygen at 450 to 550K may be adsorbed atomic oxygen. Kung [21] suggests that adsorbed atomic oxygen is evolved in an intermediate temperature range for several metal oxides. In AMO one can debate the use of the term lattice for oxygen desorbed in the 800 to 900K range especially when an amorphous material is being used, however, even an amorphous material can have a framework structure with a local ordering such as in glass. Degradation of the O atoms from tetrahedrally coordinated Si would disrupt glass [22] in much the same way as decomposition of AMO.

It is clear from other TPD studies [24,25] of desorbed oxygen with manganese oxide systems that these oxygen species are mobil and can migrate from one type of site to another especially at periods greater than 1 hour. Usually, lattice oxygen seems to migrate to lower energy sites that may be associated with atomically adsorbed O_2 and monatomic O species.

4.2. Photoassisted catalytic oxidation of isopropanol

The photoassisted catalytic oxidation of isopropanol proceeds at a large rate for AMO materials in comparison to several other photocatalysts such as TiO_2. A further advantage of AMO is that absorption can occur near 425 nm, which is far into the visible region of the spectrum. The data of Fig. 5 show that the rate of formation of acetone from isopropanol is markedly enhanced in the presence of O_2 versus N_2. The role of oxygen is not totally clear at this time, however, TPD data of Fig. 4 suggest that O needs to be replenished at the surface of AMO. Note from Fig. 4 that even at very low temperatures that there is loss of oxygen from AMO.

4.3. Photoassisted decomposition of halogenated hydrocarbons

The photoassisted catalytic oxidation data for AMO with CH_3Cl, CH_3Br and CH_3I feeds shown in Fig. 6 suggest that it is possible to degrade all three methyl halide compounds even at 5,000 ppm. This concentration regime is considerably higher than that used with TiO_2 photocatalytic systems. The data suggest that it is easier to break a C–I bond than a C–Br bond than a C–Cl bond as might be expected. The products of these photolyses are HCl, Br_2, and I_2 for CH_3Cl, CH_3Br and CH_3I, respectively. These products can be predicted on the basis of thermodynamic calculations [15]. Data of Table 1 clearly show that these rates allow efficient decomposition of methyl halides.

The fact that the rates of oxidation do not markedly change (decrease) during photolysis indicate that poisoning by halide is not as severe for AMO as it is for TiO_2 [23]. The enhanced rate of total oxidation for AMO versus TiO_2 may be related to the broad absorption (dark color versus white for TiO_2), less poisoning by halide ions, and differences in polarity of the surface which may be important during adsorption. The ability of AMO to desorb oxygen at low temperatures may also lead to enhancement in rate due to more rapid extraction of H atoms. The rate of oxygen desorption of crystalline manganese oxide materials [24,25] is much less than that of AMO.

A reviewer has questioned the use of Langmuir–Hinshelwood kinetics for treatment of such data. Dibble and Raup [27] have studied the photodegradation of trichloroethylene with TiO_2 in gas phase reactions. They observed that traditional Langmuir–Hinshelwwod–Hougen–Watson rate forms could be used to determine rates of reaction that exhibited shifts in apparent order. Their entire experimental data were not able to be fit with this model.

4.4. Effects of dopants

Dopant levels of several transition metals can be incorporated into AMO as shown by ICP analytical data. The level of dopant in these materials is extremely low, on the order of less than 0.1 per cent. Accordingly, there are no significant changes in surface area, and indeed, earlier studies of AMO materials made with different surface area show no correlation with activity in oxidation of isopropanol [13]. It is clear from the analytical composition data that extremely small amounts of dopant can have a major influence on the photooxidation activity of AMO. All of our characterization and catalytic data suggest that the electronic environment of the AMO is altered which can somewhat alter the absorption properties. The effect of the dopant ions may be to act as traps where electron transfer events are impeded.

The presence of dopants can enhance the absorption of AMO in the long wavelength region. Turnover rates for oxidation of isopropanol to acetone are markedly influenced by dopant ions. In the case of Cr^{3+} and Zn^{2+} ions, the activity is appreciably diminished as shown in Table 2. These ions may act as traps where electron transfer events are impeded. This may be related to the inability to change oxidation state (Zn^{2+}, Ni^{2+}) or unusually stable oxidation states (Cr^{3+}). For Cu^{2+}, it may be possible that reduction to Cu^{1+} occurs and that there can be a shuttling of oxidation states of copper in AMO. Further studies of the oxidation states of these ions in AMO will be necessary in order to test this hypothesis. In any event, data of Table 2 clearly show that increases and decreases in activity can occur when AMO is doped with transition metal ions.

It is clear that we do not know the oxidation states of the dopants. The level of dopant is less than 0.1 per cent. It is difficult to obtain accurate oxidation state data when such levels are so low, even with sensitive surface analytical methods such as X-ray photoelectron spectroscopy. At this stage the above thoughts concerning oxidation states are speculative, however, they are in good agreement with the observations of inorganic chemistry, and with data obtained for doped crystalline manganese oxide materials that have dopant levels that are much higher than these AMO systems.

The UV–VIS data of Fig. 8 and similar data for the other doped AMO materials suggest that the absorption profiles of the different dopants do not markedly influence the rate of photooxidation of isopropanol. These spectroscopic data and the catalytic data for the different dopants sugggest that the nature of the dopant plays a major role in determining the activity of these materials. The cation dopants that have fixed oxidation states like Ni^{2+} and Zn^{2+} are not very active. Such cations may act like traps in the electron transfer process. On the other hand, cations like Cu^{2+} which can be readily reduced to Cu^{1+} may be able to continuously allow electron transfer processes throughout the AMO material to occur, leading to higher conversions than in the other systems. This obviously does not apply to Cr^{3+} dopants, since it is difficult to obtain stable Cr^{2+} oxidation states in oxides.

5. Conclusions

We have shown here that AMO materials and doped AMO materials are active photoassisted catalysts in the selective oxidation of isopropanol to acetone and in the total oxidation of methyl halides. In all reactions, it is clear that

O_2 is necessary for regeneration of desorbed O from AMO. The dopant ions in AMO can act to enhance or diminish the rate of formation of acetone from isopropanol. Ions in fixed oxidation states appear to act as traps that decrease activity, whereas ions that can exist in mixed valent states appear to enhance activity. Thermodynamic analyses as well as product analyses suggest that in the case of CH_3Br and CH_3I that halogen gases are final products of the decomposition whereas HCl is the final product when CH_3Cl is photolyzed. These studies show that AMO is an outstanding photoassisted catalytic oxidation material for both selective and total oxidations.

Acknowledgements

We thank the Department of Energy, Office of Basic Energy Sciences, Division of Chemical Sciences for support of this research. VP acknowledges a traineeship fellowship from the Education Division of the National Science Foundation.

References

[1] V. Ramamurthy, Photochemistry in Organized and Constrained Media, VCH Publishers, New York, 1991.
[2] D.S. Wuttke, H.B. Gray, S.L. Fisher and B. Imperial, J. Am. Chem. Soc., 115 (1993) 8455–8456.
[3] K.V. Gobi and R. Ramaraj, J. Mol. Catal., 84 (1993) 187–192.
[4] N. Sutin and C. Creutz, Adv. Chem. Ser., 168 (1987) 1–27.
[5] S. Baral and J.H. Fendler, in M.A. Fox and M. Chanon, Eds., Photoinduced Electron Transfer, Part B, Elsevier Science, Amsterdam, 1988, pp. 541–563.
[6] N.J. Turro, Pure Appl. Chem., 58 (1986) 1219–1224.
[7] D. Gust and T.A. Moore, in D. Volman, G. Hammond and D.C. Neckers, Eds., Advances in Photochemistry, Vol. 16, Wiley, NY, 1991.
[8] A. Helms, D. Heiler and G. McLendon, J. Am. Chem. Soc., 114 (1992) 6227–6238.
[9] M. Gratzel and Kalyanasundaram, Eds., Kinetics and Catalysis in Microheterogeneous Systems, Marcel Dekker, NY, 1991.
[10] V. Balzani and F. Scandola, Supramolecular Photochemistry, Ellis Hardwood, NY, 1991.
[11] S.L. Suib, Chem. Rev., 93 (1993) 803–826.
[12] G.A. Waychunas, Rev. Min., Min Soc. Am., 25 (1991) 11–68.
[13] H. Cao and S.L. Suib, J. Am. Chem. Soc., 116 (1994) 5334–5342.
[14] J.F. Tanguay, S.L. Suib and R.W. Coughlin, J. Catal. 117 (1989) 335–347.
[15] J.C. Lin, Masters Thesis, University of Connecticut, Storrs, 1995.
[16] J.W. Murray, L.S. Balistieri and B. Paul, Geochim. Cosmochim. Acta, 48 (1984) 1237–1242.
[17] Y.F. Shen, R.P. Zerger, R. De Guzman, S.L. Suib, L. McCurdy, D.I. Potter and C.L. O'Young, Science, 260 (1993) 511–515.
[18] S. Ching, J.A. Landrigan, M.L. Jorgensen, N. Duan, S.L. Suib, and C.L. O'Young, Chem. Mater., 7 (1995) 1604–1606.
[19] R.N. DeGuzman, Y.F. Shen, E.J. Neth, S.L. Suib, C.L. O'Young, S. Levine and J.M. Newsam, Chem. Mater., 6 (1994) 815–821.
[20] M. Anpo, S.C. Moon and K. Chiba, Res. Chem. Intermed., 19 (1993) 495–502.
[21] H.H. Kung, Transition Metal Oxides, Surface Chemistry and Catalysis, Elsevier Science, Amsterdam, 1989, pp. 110–120.
[22] M.H. Lewis, Glasses and Glass Ceramics, Chapman and Hall, London, 1989.
[23] (a) L.A. Dibble and G.B. Raupp, Env. Sci. Technol., 26 (1992) 492–498; (b) J.D. Freihaut, P. Bonczyk, J. Sangiovanni and B. Woody, UTRC Interim Report R93-491211-1, September 1, 1993.
[24] Y.G. Yin, W.Q. Xu, R. DeGuzman, S.L. Suib and C.L. O'Young, Inorg. Chem., 33 (1994) 4384–4389.
[25] Y.G. Yin, W.Q. Xu, S.L. Suib and C.L. O'Young, Inorg. Chem., 34 (1995) 4187–4193.
[26] D.F. Ollis, C.Y. Hsiao and C.L. Lee, J. Catal., 82 (1983) 418–423.
[27] L.A. Dibble and G.B. Raupp, Catal. Lett., 4 (1990) 345–351.